Int J Ind Chem (2016) 7:167–180
DOI 10.1007/s40090-015-0066-4

RESEARCH

Biosorption of cationic dye from aqueous solutions onto lignocellulosic biomass (*Luffa cylindrica*): characterization, equilibrium, kinetic and thermodynamic studies

Noureddine Boudechiche[1] · Hassiba Mokaddem[1] · Zahra Sadaoui[1] · Mohamed Trari[2]

Received: 16 June 2015 / Accepted: 22 November 2015 / Published online: 22 January 2016

Abstract In the present study, biomass fiber (*Luffa cylindrica*) has been successfully used as biosorbent for the removal of a cationic dye namely, methylene blue, from aqueous solution using a batch process. The characterization of the biosorbent was carried out by the infrared spectroscopy (FTIR) and scanning electron microscopy (SEM). The chemical composition has been established by the energy dispersive X-Ray spectroscopy (EDS). The effects of various parameters such as the contact time (0–160 min), solution pH (2–10), biosorbent dose (0.5–8 g L^{-1}), particle size, initial MB concentration (20–300 mg L^{-1}) and temperature (20–60 °C) were optimized. The biosorption isotherms were investigated by the Langmuir, Freundlich, Dubinin–Radushkevich and Tempkin models. The data were well fitted with the Langmuir model, with a maximum biosorption capacity of 49.46 mg g^{-1} at 20 °C. The kinetics data were analyzed by the pseudo-first-order and pseudo-second-order models. The mass transfer model in terms of interlayer diffusion was applied to examine the mechanisms of the rate-controlling step ($R^2 = 0.9992$–0.9999). The thermodynamic parameters: free energy ($\Delta G° = -5.428$ to -3.364 kJ mol^{-1}), enthalpy ($\Delta H° = -20.547$ kJ mol^{-1}) and entropy ($\Delta S° = -0.052$ kJ mol^{-1} K^{-1}) were determined over the temperatures range (20–60 °C). The results indicate that *Luffa cylindrica* could be an interesting biomass of alternative material with respect to more costly adsorbents used nowadays for dye removal.

Keywords Biosorption · *Luffa cylindrica* · Methylene blue · Characterization · Kinetic · Isotherm

Introduction

Dyes are widely used in various industries such as textile, leather, paper, printing, food, cosmetics, paint, pigments, petroleum, solvent, rubber, plastic, pesticide, wood preserving chemicals, and pharmaceutical industry. Over 10,000 of different commercial dyes and pigments exist currently and more than 7×10^5 tonnes are produced annually worldwide [1–3]. Discharge of dye-bearing wastewaters into the natural environment from textile, paper and leather industries causes a serious threat for the aquatic life [4]. On the other hand, limited aquatic resources and increasing demand for safe water require efficient water treatment methods [5]. Synthetic dyes are generally resistant to biodegradation and physicochemical techniques for their removal [6, 7], such as adsorption, chemical oxidation, electrocoagulation and advanced oxidation processes (AOPs) have been extensively used to comply with more and more stringent legislation regarding the maximum allowable dye concentration in wastewaters [7–10]. Methylene blue (MB) is a thiazine cationic dye with widespread applications, including coloring paper, dyeing cottons, wools and coating for paper stock. It is also used in microbiology, surgery and diagnostics and as a sensitizer in photo-oxidation of organic pollutants. Although it has low toxicity, it can cause some specific harmful effects for the human health such as heartbeat

✉ Mohamed Trari
solarchemistry@gmail.com

[1] Laboratory of Engineering Reaction, Faculty of Engineering Mechanic and Engineering Processes, USTHB, BP 32, Algiers, Algeria

[2] Laboratory of Storage and Valorization of Renewable Energies, Faculty of Chemistry, USTHB, BP 32, Algiers, Algeria

increase, vomiting, shocks, cyanosis, jaundice and tissue necrosis [11, 12]. Hence, its removal from wastewaters is an important issue for the environmental protection [13]. The conventional methods have been extensively used for treating waters contaminated with heavy metal and dyes [14–16]. However, these methods present some disadvantages such as high cost, low removal efficiency and production of excessive toxic sludge [17]. Recently, inexpensive, ecofriendly and not pathogenic organisms have been used for the dye removal [18]. In this respect, the biosorption process has attracted a great interest in this context, and seems a good alternative for the removal of dyes and other pollutants from wastewaters [19, 20], as a replacement for costly commercially biosorbents [21]. It can be defined as sequestering of organic or inorganic compounds by alive or dead biomasses or their derivatives; the biomass can consist of bacteria [22], fungal [19], yeasts [22], algae [23], seaweeds and even industrial or agricultural wastes [24, 25]. Different vegetal biomasses have been used such as Opuntia ficus indica [26], Sugar beet pulp [21], Stoechospermum marginatum [24], *Scolymus hispanicus* L. [27], Palm kernel [28], Pinus brutia Ten. [29], Waste orange peel [30], Posidonia oceanica L. [31], Cyperus rotundus [32], Date stones and Palm-trees waste [33].

The present study examines a new dye biosorbent namely the *Luffa cylindrica* fiber and its feasibility for the removal of methylene blue from aqueous solution. It is inexpensive and easily available in many regions of Algeria. *Luffa cylindrica* is composed of 60 % cellulose, 30 % hemicelluloses and 10 % lignin and is classified as lignocellulosic material [34]; the *Luffa* products are natural and biodegradable. The biosorption of methylene blue onto *Luffa cylindrica* fiber is carried out by batch biosorption experiments. The influence of the contact time, initial pH, biosorbent dose, initial MB concentration, particle size and temperature is investigated. Furthermore, the isotherm and kinetic models are evaluated and the thermodynamic data are determined.

Materials and methods

Preparation of the biosorbent

The *Luffa cylindrica* plant was naturally collected in July, from Algeria. The plant was repeatedly washed with distilled water to remove dirt particles, dried at 80 °C for 48 h, crushed in grinder and sieved to obtain particle sizes in the range (63–630 µm). The powdered biosorbent was stored in an airtight container until use.

Point of zero charge (pH_{pzc})

The point of zero charge (pH_{pzc}) of the *Luffa cylindrica* fiber was evaluated by the solid addition method using KNO_3 (0.01 M) solution [36]. The experiments were carried out in 100 mL erlenmeyer flasks with stopper cork containing 50 mL of KNO_3 solution (10^{-2} M). The initial pH (pH_i) in each flask was adjusted between 3 and 11 by adding NaOH or HCl solutions (0.1 M). Then, 0.5 g of the *Luffa cylindrica* was added to each flask which are kept for 48 h with intermittent manual shaking to reach the equilibrium. The difference of the initial and final pH (pH_i, pH_f) was plotted against the initial pH. The point of intersection of the resulting curve with the abscissa axis, for which $\Delta pH = 0$, gives pH_{pzc} (Fig. 1).

Methylene blue solution

The dye used in all experiments was methylene blue, a basic cationic dye supplied by (Biochem company, Algeria). MB was chosen because of its various applications. MB has a molecular weight of 319.85 g mol^{-1}, which corresponds to methylene blue hydrochloride with three water molecules, the structure is shown in Fig. 2.

The FT-IR spectra were recorded over the range (400–4000 cm^{-1}) using a Shimadzu FTIR-8400S spectrometer. The scanning electron microscopy (SEM) was performed with a JEOL-JSM 6360 Microscope.

Batch biosorption experiments

The biosorption was conducted in Pyrex 500 mL conical flasks at a constant agitation speed. The experiments were carried out by varying the biosorbent particle size over the range (63–630 µm), contact time (5–160 min), biosorbent dosage (0.5–8 g L^{-1}), pH (2–10), initial dye concentrations (20–300 mg L^{-1}) and temperatures (20–60 °C). The

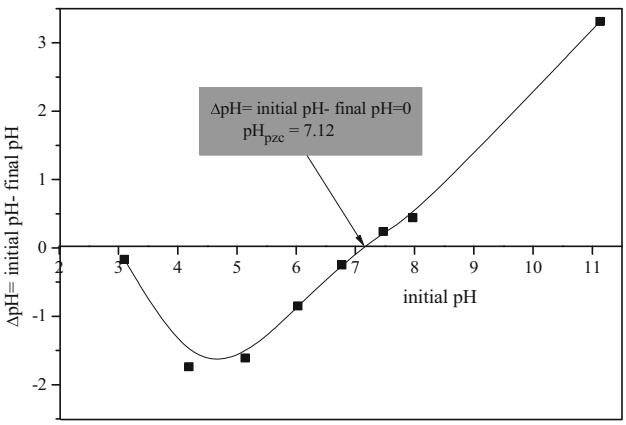

Fig. 1 The chemical structure of the methylene blue

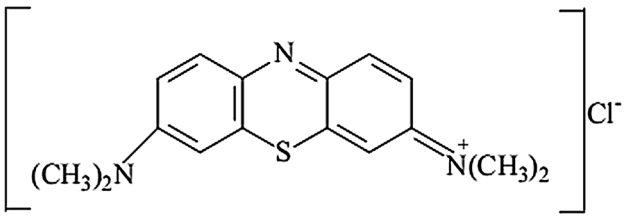

Fig. 2 The determination of the point of zero charge (pH_{PZC})

temperature was controlled with an isothermal shaker. After each biosorption test, the sample was centrifugated (6000 rpm, 10 min) for solid–liquid separation; the residual MB concentration was analyzed by a UV–Vis spectrophotometer (2120 UV Optizen III, South Korea) at $\lambda_{max} = 663$ nm. The equilibrium, kinetic and thermodynamic study were performed by determining the optimum biosorption conditions. The amount of MB biosorbent q_t (mg g^{-1}) was calculated from the relation (1):

$$q_t = \frac{(C_0 - C_t)}{m} V \quad (1)$$

where C_0 is the initial dye concentration (mg L^{-1}), C_t the concentration of dye at time t (mg L^{-1}), V the volume of the solution (L) and m the mass of biosorbent (g). The dye removal percentage is calculated as:

$$R\,(\%) = \frac{(C_0 - C_t)}{C_0} 100 \quad (2)$$

Statistical evaluation of the kinetic and isotherm parameters

To determine the best-fit model for the biosorption, the linear curve fitting by the software OriginPro 8.5 was employed to simulate and to confirm the fitting of the biosorption kinetic and isotherm models to the experimental data. The statistical significance of variables was evaluated from the analysis of variance ANOVA (Fisher function, F value, and probability, P value), while the adjusted correlation coefficient (Adjusted R^2) was used to assess the adequacy of the fitting [35]. F value and Adjusted R^2 were calculated as:

$$F \text{ value} = \frac{\left(\sum_{i=1}^{n} \left(q_{i,cal} - \bar{q}_{i,\exp}\right)^2\right)/p - 1}{\left(\sum_{i=1}^{n} \left(q_{i,\exp} - q_{i,cal}\right)^2\right)/n - p} \quad (3)$$

$$\text{Adjusted } R^2 = 1 - \frac{\left(\sum_{i=1}^{n} \left(q_{i,\exp} - q_{i,cal}\right)^2\right)/n - p}{\left(\sum_{i=1}^{n} \left(q_{i,\exp} - \bar{q}_{i,\exp}\right)^2\right)/n - 1} \quad (4)$$

where $q_{i,exp}$ is each value of q_i measured experimentally, $q_{i,cal}$ is each value of q_i predicted by the fitted model, $\bar{q}_{e,exp}$ is the average of q_i experimentally measured, n is the number of experiments performed and p is the number of parameter of the fitted model.

Desorption

MB solution (100 mg L^{-1}) was mixed with *Luffa cylindrica* at pH 6 for 4 h. The residual MB concentration was measured. The MB loaded *Luffa cylindrica* was dried at 80 °C. Four eluting solvents (100 mL): H_2O, HCl (0.1 M), NaOH (0.1 M), and NaCl (0.1 M) each one containing 0.2 g of MB loaded *Luffa cylindrica* at room temperature. The percentage of desorbed dye from the adsorbent was calculated (=100× desorbed mass/adsorbed mass).

Results and discussion

Characterization

FT-IR analysis of the biosorbent

The FT-IR spectrum of the *Luffa cylindrica* was plotted to obtain information about the nature of functional groups at the surface. The spectrum (Fig. 3) shows a dominant peak at 3450 cm^{-1} attributed to O–H stretching vibrations in hydroxyl groups, involved in hydrogen bonds. The bands observed at 2944 cm^{-1} are assigned to asymmetric C–H bonds, present in alkyl groups. The absorption peaks at 1737 cm^{-1} correspond to stretching of carboxyl groups. The strong absorption band at 1639 cm^{-1} is indicative of OH bending vibrations, while that at 1401 cm^{-1} is due to C–O stretching. The band at 1322 cm^{-1} is assigned to C–O groups on the biomass surface, whereas that at 1160 cm^{-1} corresponds to antisymmetric bridge C–OR–C stretching

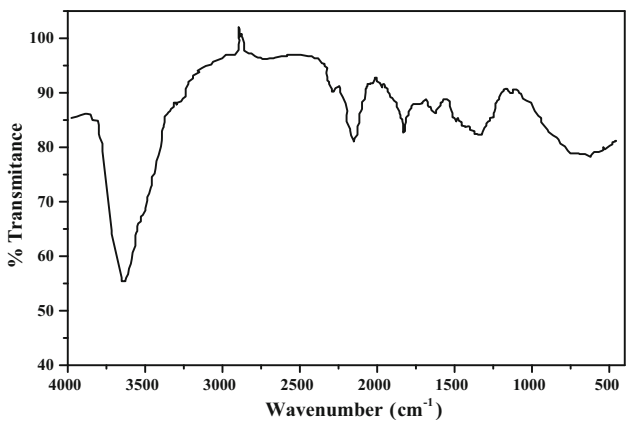

Fig. 3 FTIR spectrum of *Luffa cylindrica*

(cellulose) [37, 38]. The band at 1107 cm^{-1} is attributed to anhydroglucose ring (cellulose) [38]. The peaks at 1058 cm^{-1} are indicative of C-OR stretching (cellulose), while the band at 884 cm^{-1} could be attributed to antisymmetric, out of phase ring stretching [37].

SEM–EDS analysis

The morphology of the *Luffa cylindrica* was observed by SEM. The fibers, formed by fibrils glued, are disposed in a multi-directional array, forming a natural mat (Fig. 4a); the diameters of single fibers are in the range (63–125 μm). To observe the inner fibrils and further investigate the complicated physical structures in the natural *Luffa cylindrica*, a crude fiber was observed at high magnification (Fig. 4b). The SEM image shows that the fiber has a heterogeneous appearance with an outer rich lignin layer around the fibers. The internal fibrils cannot be seen due to the lignin layer. At higher magnification (Fig. 4c, d), the SEM image displays a rougher surface with lots of waxy and gummy substances on the untreated *Luffa cylindrica* fiber; the internal fibrils cannot be observed [38]. The EDS spectrum is shown in Fig. 5 and the contents of each element are listed in Table 1. The energy dispersive X-Ray microanalysis (SEM/EDS) of the *Luffa cylindrica* fibers indicates mainly the presence of carbon (65.68 %) and oxygen (30.13 %). However, as the EDS analysis is less sensitive for light elements ($Z \leq 10$) [39], the carbon and oxygen content were quantified by ultimate analysis. Their concentrations suggest the presence of high amount of different oxygenated groups on the carbon surfaces, such as Cl, Ca, Na, Cu, Mg, K, Ni, Si and P whose contents are between 0.09 and 1.21 %. Similar results (carbon: 64.0 %, oxygen: 34.9 %) were already obtained by Tanobe et al. [38].

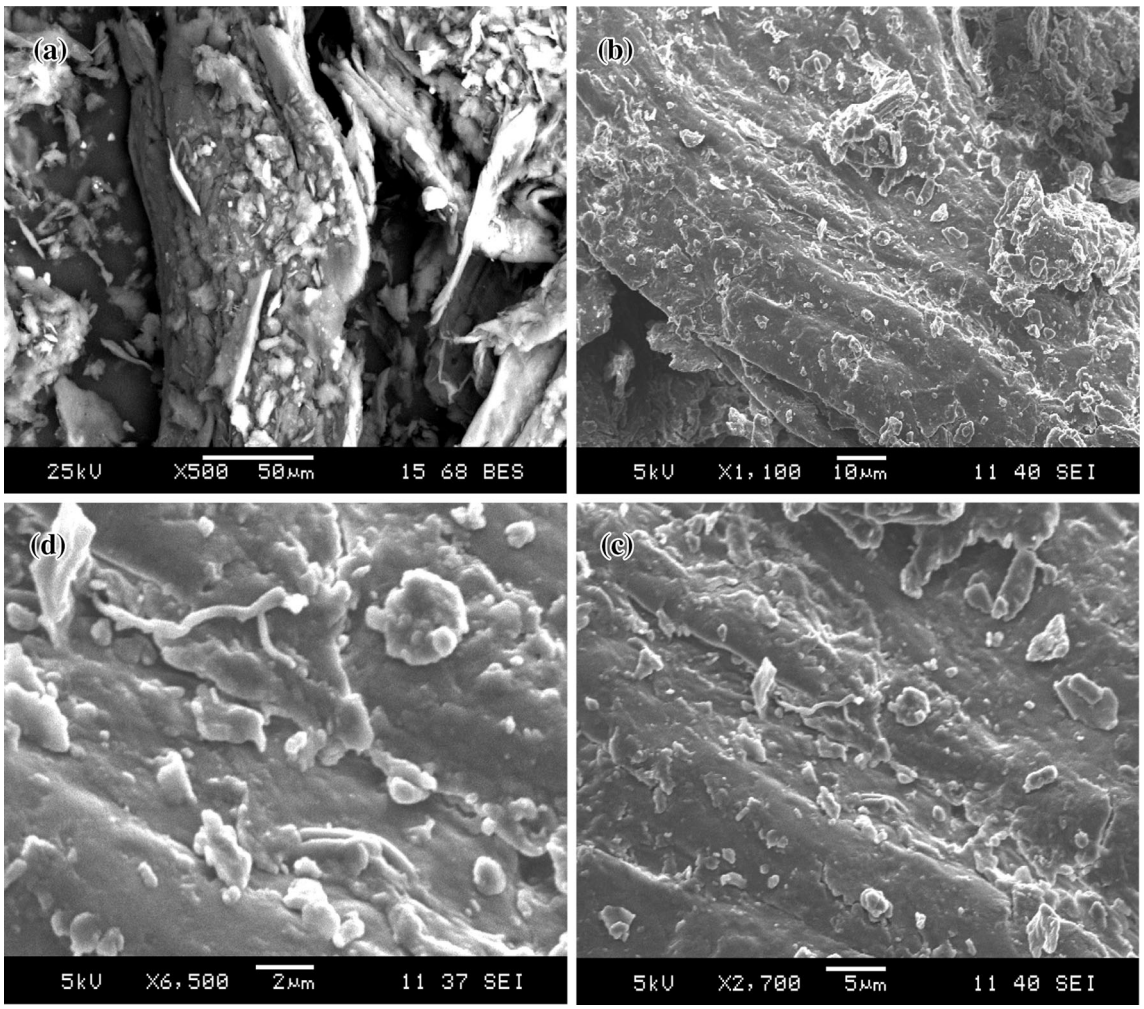

Fig. 4 SEM micrographs of *Luffa cylindrica*

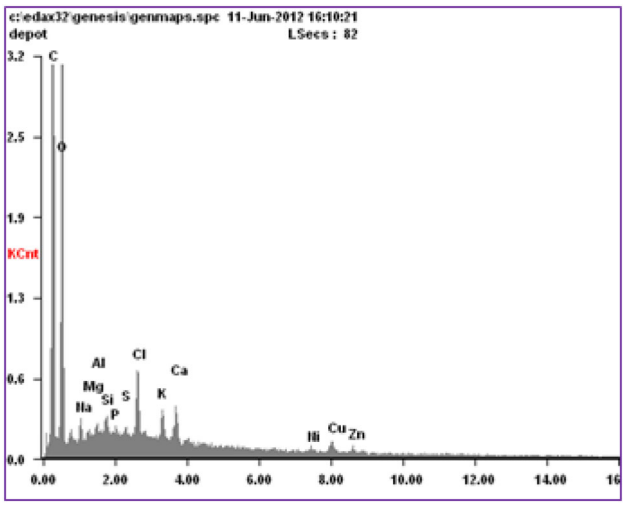

Fig. 5 EDS spectrum from the *Luffa cylindrica*

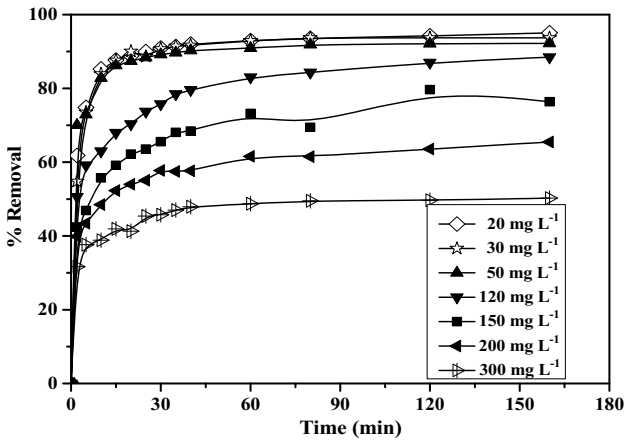

Fig. 6 Effect of contact time on the biosorption kinetics of MB by *Luffa cylindrica* (biosorbent dose = 3 g L^{-1}, initial pH = 5.80 and $T = 20$ °C)

Biosorption

Effect of contact time and initial dye concentration

Experiments were undertaken to study the effect of the initial concentration of MB over the range (20–300 mg L^{-1}) at 20 °C on the biosorption onto *Luffa cylindrica* at regular interval times. The rate of the MB removal by *Luffa cylindrica* was rapid, the maximum uptake was achieved in the first 20 min, accounting for 90–42 % biosorption, respectively, for MB initial concentrations of 20–300 mg L^{-1} (Fig. 6). The biosorption rate after this initial fast phase slows down significantly until it reaches a plateau after 60 min, indicating equilibrium of the system. The initial rapid phase may be due to an increase in the number of available vacant sites. The increase of the biosorption with raising the MB concentration is attributed to the fact that at higher concentrations, the ratio of the initial number of MB molecules to the available surface area is large; consequently, the fractional biosorption becomes dependent on the initial concentration. By contrast, at low concentrations, the available sites of biosorption are fewer and hence the MB removal depends upon their concentration [40].

Effect of solution pH

The pH of the solution is a crucial controlling parameter in the biosorption [41, 42]. This is possibly due to its impact on both the surface binding sites of the biosorbent and ionization status of the MB molecule in water. Since the MB biosorption can dramatically change with changing pH, it has been stressed that not only it should be accurately reported but also the data for all comparative studies must be obtained at the same pH values. The effect of pH on MB biosorption was studied over the pH range (2–10) and the results are shown in Fig. 7. The equilibrium biosorption uptake presents a minimum at pH ~ 2 (6.16 %) and increases up to 5, then remains nearly constant (80.86 %) over the initial pH ranges (6–10). At low pHs, the surface charge is positively charged, and the H^+ ions compete effectively with dye cations causing a decrease in the amount of adsorbed dye. At higher pH, the *Luffa cylindrica* fibers, mainly lignin and cellulose chains, become negatively charged, thus enhancing the cationic dye by electrostatic attraction forces [43, 44].

Effect of biosorbent dose

The biosorbent dose is an important parameter because it determines the capacity of biosorbent for a given concentration of the adsorbate [45]. The effect of the biomass dosage (0.5–8 g L^{-1}) on the MB biosorption was studied in 1 L MB solution (50 mg L^{-1}) under optimized conditions of pH and contact time. The removal percentage of MB increases drastically from 12.77 to 96.16 % for biosorbent dosage of 0.5 and 8 g L^{-1}, respectively (Fig. 8). This is due to the availability of more binding sites as the dose of biosorbent increases. It is due to the high number of unsaturated biosorption sites during the biosorption process

Table 1 Principal elements identified on the biomass surface by SEM/EDS

Element	C	O	Na	Mg	Si	P	Cl	K	Ca	Ni	Cu
Content (%)	65.68	30.13	0.71	0.19	0.11	0.09	1.21	0.36	0.77	0.16	0.50

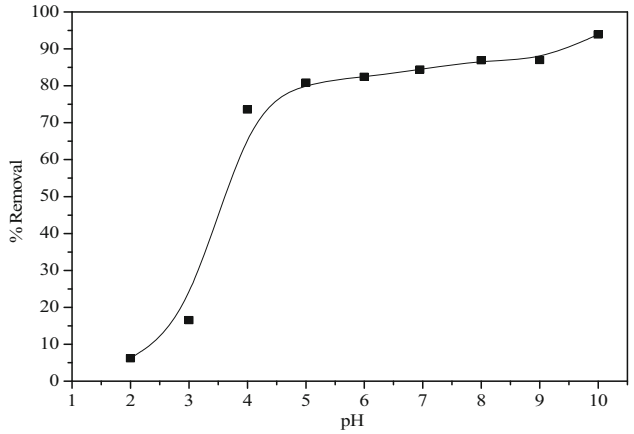

Fig. 7 Effect of the solution pH on the MB removal ($C_0 = 20$ mg L^{-1}, biosorbent dose = 1 g L^{-1} and $T = 20$ °C)

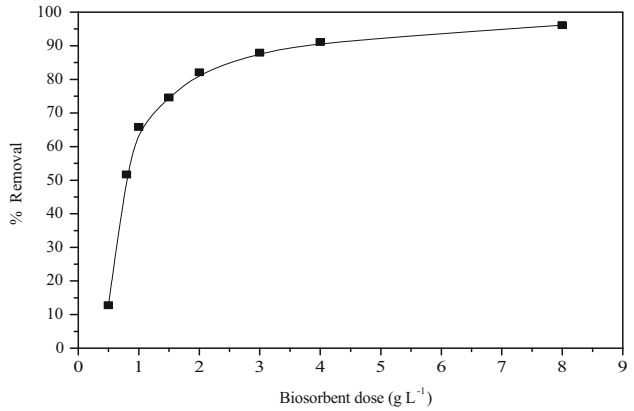

Fig. 8 Effect of the biosorbent dose on the MB biosorption by *Luffa cylindrica* ($C_0 = 20$ mg L^{-1}, initial pH 5.80 and $T = 20$ °C)

[46]. Similar results were previously reported by some researchers [45, 47].

Effect of biosorbent particle size

The particle size of the biosorbent can greatly influence the external surface of the biosorbent, thus impacting on its interaction with the solution through the effect of resistance to the film diffusion. As a consequence, a variation in the biosorbent particle size modifies the accessibility and the availability of reactive groups present on its surface [13]. The biosorption of MB was studied at four different domains (63–125, 125–250, 250–400 and 400–630 µm) of the biomass fibers. As expected, it was found that the MB biosorption decreases with increasing the size of the biosorbent (Fig. 9). This is due to larger surface area of smaller particles for the same amount of the biosorbent. For larger particles, the diffusion resistance to the mass transport is higher, and most of the internal surface of the

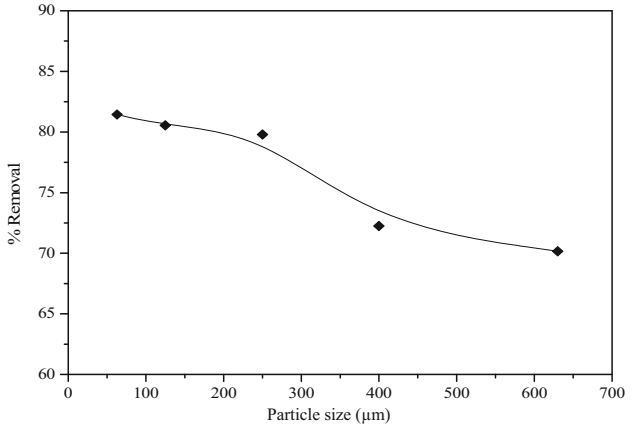

Fig. 9 Effect of the particule size on the MB removal ($C_0 = 10$ mg L^{-1}, initial pH 5.80, biosorbent dose = 0.5 g L^{-1} and $T = 20$ °C)

particle is not utilized for biosorption. Consequently, the amount of MB adsorbed is small. Similar results were reported by other researchers with coniferous brown macroalga Stoechospermum marginatum [24] and *Scolymus hispanicus* L. [27], Pinus brutia Ten. [29].

Effect of temperature

The temperature is well known to play an important role in the biosorption process [48]. The biosorption of MB on *Luffa cylindrica* fiber was investigated over the range (20–60 °C). A slight decrease in the dye biosorption with raising temperature was observed from Fig. 10, suggesting an exothermic process.

Biosorption isotherms

The isotherm describes the equilibrium between the concentration of the adsorbate on the solid phase and the concentration in the liquid phase. The equilibrium biosorption data have been analyzed using the Langmuir,

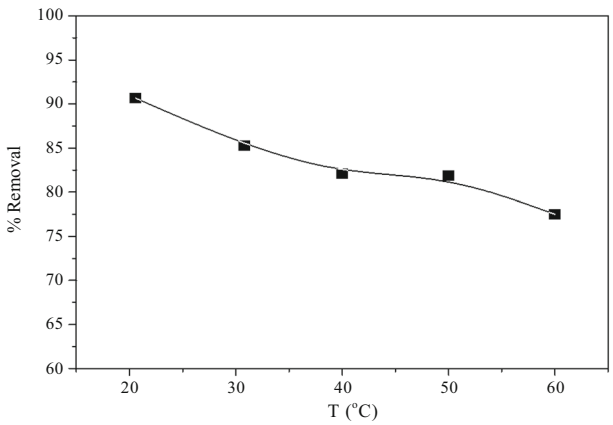

Fig. 10 Effect of the temperature on the MB biosorption ($C_0 = 50$ mg L^{-1}, initial pH 5.80, and biosorbent dose = 0.5 g L^{-1})

Table 2 Constants of isotherm models for the biosorption of MB onto *Luffa cylindrica* fiber at various initial MB concentrations

Langmuir				
K_L (L mg^{-1})	q_{max} (mg g^{-1})	R^2	F value	P value
0.120	49.456	0.9969	1899.657	1.200×10^{-7}
Tempkin				
A_T (L mg^{-1})	b_T (J mol^{-1})	R^2	F value	P value
2.049	276.986	0.9591	141.613	7.383×10^{-5}
Freundlich				
K_F (mg g^{-1}) (mg L^{-1}) $^{-1/nF}$	n_F	R^2	F value	P value
7.572	2.342	0.8957	52.522	7.811×10^{-4}
Dubinin–Radushkevich (D–R)				
E (kJ mol^{-1})	q_{D-R} (mg g^{-1})	R^2	F value	P value
0.968	31.838	0.7201	16.438	0.978×10^{-2}

Freundlich, Dubinin–Radushkevich and Tempkin models. Such analysis is important to develop a relation that accurately represents the experimental results and could be used for design purposes [49].

The Langmuir model is based on an the assumption that the biosorption occurs on specific homogeneous sites of the biosorbent and the monolayer biosorption onto a surface containing a finite number of uniform sites with no trans-migration of adsorbate in the plane of the surface [50]; the isotherm is expressed by Eq. (5).

$$q_e = \frac{q_{max} K_L C_e}{(1 + K_L C_e)} \tag{5}$$

where C_e is the equilibrium dye concentration (mg L^{-1}), q_e the amount of biosorbed dye (mg g^{-1}), q_{max} the amount for a complete biosorption monolayer (mg g^{-1}), and K_L the constant related to the affinity of the binding sites and energy of biosorption (L mg^{-1}).

$$\frac{C_e}{q_e} = \frac{1}{q_{max} K_L} + \frac{C_e}{q_{max}} \tag{6}$$

A dimensionless constant separation factor (R_L) of the Langmuir isotherm was used to determine the favorability of the biosorption process. R_L is defined using Eq. (7); its value indicates the type of isotherm: irreversible ($R_L = 0$), favorable ($0 < R_L < 1$), linear ($R_L = 1$) or unfavorable ($R_L > 1$) [50].

$$R_L = \frac{1}{(1 + K_L C_0)} \tag{7}$$

The Freundlich expression is an empirical equation based on the biosorption onto a heterogeneous surface. The equation generates an exponential shaped theoretical equilibrium curve [51] and is represented as follows:

$$q_e = K_F C_e^{\frac{1}{nF}} \tag{8}$$

$$\ln q_e = \ln K_F + \frac{1}{n_F} \ln C_e \tag{9}$$

where K_F (mg g^{-1} L$^{(1/n)}_F$ mg$^{-(1/n)}_F$) is the Freundlich constant and ($1/n_F$) the heterogeneity factor, related to the capacity and the biosorption intensity.

The Dubinin–Radushkevich (D–R) model does not assume a homogeneous surface or a constant biosorption potential [52]. The biosorption characteristic is related to the porous structure of the biosorbent [53].

$$q_e = q_{D-R} \exp(-\beta \varepsilon^2) \tag{10}$$

The Polanyi potential (ε) is equal to:

$$\varepsilon = RT \ln\left(1 + \frac{1}{C_e}\right) \tag{11}$$

where ε is a constant related to the mean free energy of biosorption per mole of biosorbate (mol^2 J^{-2}), q_{D-R} (mg g^{-1}) the theoretical saturation capacity, R (J mol^{-1} K^{-1}) is the universal gas constant, and T (K) the absolute temperature.

The energy E is defined as the free energy change (kJ mol^{-1}), required to transfer 1 mol of ions from the solution to the solid:

$$E = (2\beta)^{-1/2} \tag{12}$$

$$\ln q_e = \ln q_{D-R} - \beta \varepsilon^2 \tag{13}$$

Tempkin and Pyzhev have considered the effects of indirect adsorbate/adsorbate interactions on the biosorption isotherms and suggested that the heat of biosorption of all molecules on the layer should decrease linearly with the coverage [26]. The Temkin isotherm is shown in Eq. (14) [54, 55]:

$$q_e = \left(\frac{RT}{b_T}\right) \ln(A_T C_e) \tag{14}$$

Equation (14) can be expressed in its linear form :

$$q_e = \frac{RT}{b_T} \ln(A_T) + \frac{RT}{b_T} \ln(C_e) \tag{15}$$

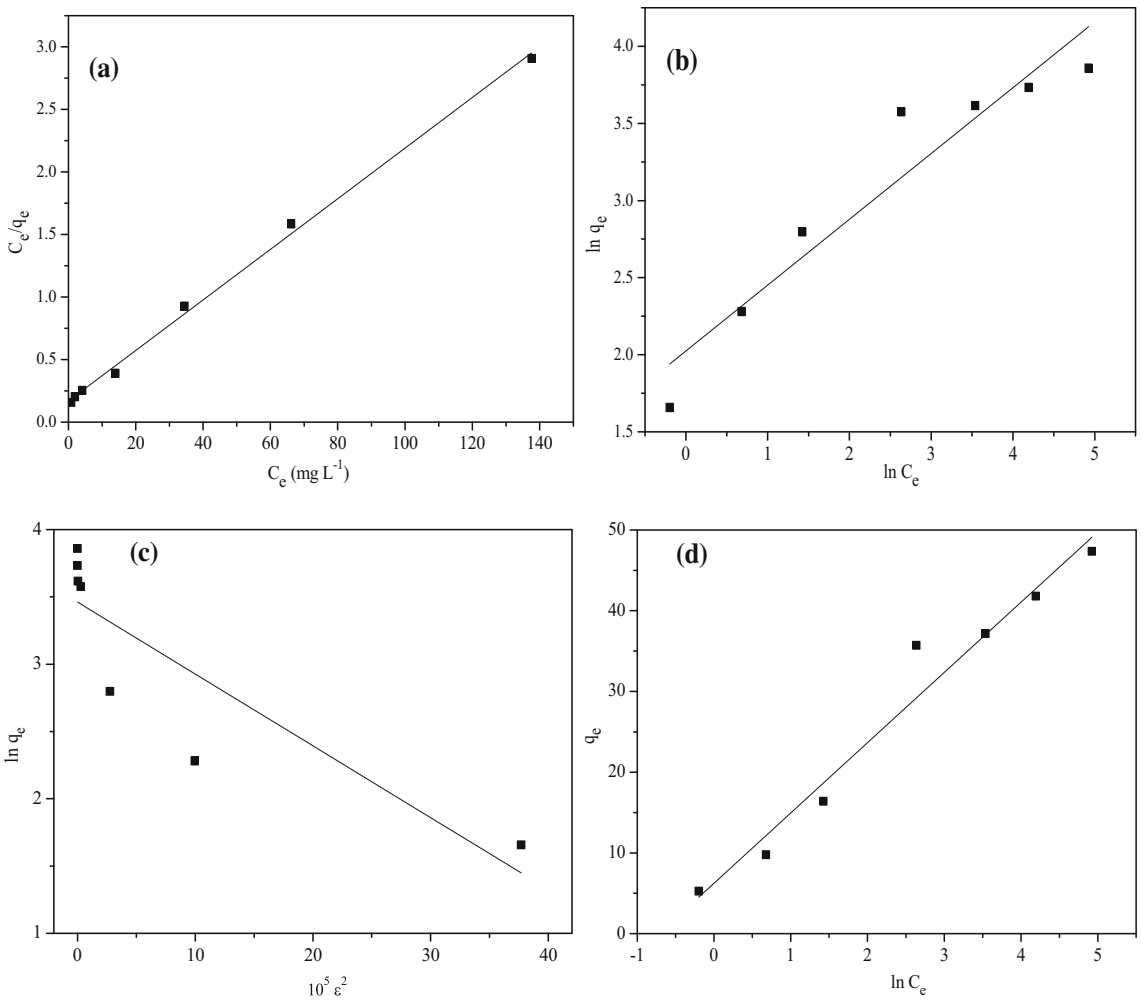

Fig. 11 The isotherm plots: Langmuir biosorption isotherm (**a**), Freundlich biosorption isotherm (**b**), Dubinin–Radushkevich (**c**) and Tempkin biosorption isotherm (**d**)

Table 3 Comparison of the maximum biosorption capacity of dyes for different absorbents

Absorbents	Adsorbates	q_{max} (mg g^{-1})	References
Raw *Luffa cylindrica*	MB	49.46	Present work
Activated *Luffa cylindrica* by NaOH (0.1 M)	MB	49	[57]
Lignite	MB	41.49	[58]
Activated *Luffa cylindrica* by H_3PO_4 (20 %) and $ZnCl_2$ (50 %)	Reactive Orange	38.31	[59]
Activated *Luffa cylindrica* by NaOH (2 %)	Malachite Green	29.4	[60]
Olive stone	MB	13.2	[61]
Defatted *Scenedesmus* sp. biomass	MB	7.73	[62]
Wood millet carbon	MB	4.94	[63]
Activated peanut stick	MB	2.54	[64]

where A_T is the equilibrium binding constant corresponding to the maximum binding energy (L mg^{-1}) and b_T (J mol^{-1}) the Tempkin isotherm constant related to the heat of biosorption.

The biosorption isotherms are useful to describe the interaction adsorbate/biosorbent of any system. The parameters obtained from different models provide information on the biosorption mechanisms, the surface properties and

affinities of the biosorbent [56]. Table 2 and Fig. 11 illustrate the isotherms for 160 min of contact time, initial MB concentration in the range (20–300 mg L^{-1}), a pH of 5.80, a biosorbent dose of 3 g L^{-1} and a temperature of 20 °C. Based on the linear regression correlation coefficient (R^2), F and P values, the isotherm models fit well the experimental data in the following order:

- Langmuir R^2 > Tempkin R^2 > Freundlich R^2 > (D–R) R^2.
- Langmuir F value > Tempkin F value > Freundlich F value > (D–R) F value.
- Langmuir P value < Tempkin P value < Freundlich P value < (D–R) P value.

Table 3 presents the comparison of the maximum biosorption capacity (q_{max}) of MB onto *Luffa cylindrica* fiber with those obtained by other researchers. It is clear that the *Luffa cylindrica* used in this work without any treatment has a relatively suitable biosorption capacity compared to other biosorbents in the literature. Therefore, raw *Luffa cylindrica* fibers seem to be competitive to other methylene blue sorbents and some optimizing treatments on this biomass might be interesting for further studies.

Biosorption kinetics

The kinetic is important for understanding the treatment of aqueous solutions because it provides valuable information about the mechanism of biosorption processes and potential rate-controlling steps, such as the mass transport [56]. Experimental data of MB biosorption using *Luffa cylindrica* fibers were evaluated by the pseudo-first and pseudo-second-order kinetics and intra-particle diffusion models to understand the mechanisms of the biosorption process.

The pseudo-first-order rate expression of Lagergren [65] is generally described by the following equation [66]:

$$\log (q_e - q_t) = \log q_e - \frac{k_1 t}{2.303} \quad (16)$$

where q_e and q_t are the amounts of dye adsorbed at equilibrium and at time t (mg g^{-1}), respectively, and k_1 the pseudo-first-order rate constant (min^{-1}), k_1 is obtained from the slope of the linear plot of log ($q_e - q_t$) against t.

The pseudo-second-order kinetic model is expressed as [67]:

$$\frac{t}{q_t} = \frac{1}{k_2 q_e^2} + \frac{1}{q_e} t \quad (17)$$

where k_2 is the rate constant of second-order biosorption (g mg^{-1} min^{-1}). If the second-order kinetic is applicable, the plot of t/q_t against t of Eq. (17) should give a linear plot. The initial biosorption rate "h" (mg g^{-1} min^{-1}) is expressed as [68]:

Table 4 Kinetic parameters for the biosorption of MB onto *Luffa cylindrica* fiber at various initial MB concentrations

C_0 (mg L^{-1})	$q_{e,exp}$ (mg g^{-1})	Pseudo-first order					Pseudo-second-order					Intra-particle diffusion		
		k_1 (min^{-1})	q_e theo (mg g^{-1})	R^2	F value	P value	k_2 (g mg^{-1} min^{-1})	h (mg g^{-1} min^{-1})	q_e theo (mg g^{-1})	R^2	F value	P value	k_{int} (mg g^{-1} $min^{-1/2}$)	C (mg g^{-1})	R^2
20	5.243	2.754×10^{-2}	0.878	0.8118	48.439	3.901×10^{-5}	1.294×10^{-1}	3.600	5.274	0.9999	390658.062	0	0.736	2.407	0.9807
30	9.780	6.119×10^{-2}	1.431	0.8860	70.915	3.013×10^{-5}	7.918×10^{-2}	7.727	9.879	0.9999	449105.026	0	1.730	3.457	0.9228
50	16.387	4.535×10^{-2}	1.526	0.9634	290.858	1.012×10^{-8}	5.175×10^{-2}	14.114	16.515	0.9999	654225.822	0	0.305	14.162	0.9862
120	35.705	2.653×10^{-2}	2.984	0.9753	435.846	1.410×10^{-9}	6.017×10^{-3}	7.980	36.417	0.9992	14246.969	0	2.123	18.955	0.9913
150	37.165	2.517×10^{-2}	3.002	0.7352	28.760	4.546×10^{-4}	5.241×10^{-3}	7.753	38.462	0.9992	3300.665	0	1.990	21.034	0.9857
200	41.793	2.117×10^{-2}	2.950	0.9201	127.592	5.149×10^{-7}	5.736×10^{-3}	10.229	42.230	0.9964	11448.789	5.44×10^{-15}	2.058	25.293	0.9316
300	47.372	2.754×10^{-2}	3.251	0.8937	93.484	2.163×10^{-6}	5.148×10^{-3}	12.003	48.286	0.9999	32124.553	0	2.427	28.789	0.9668

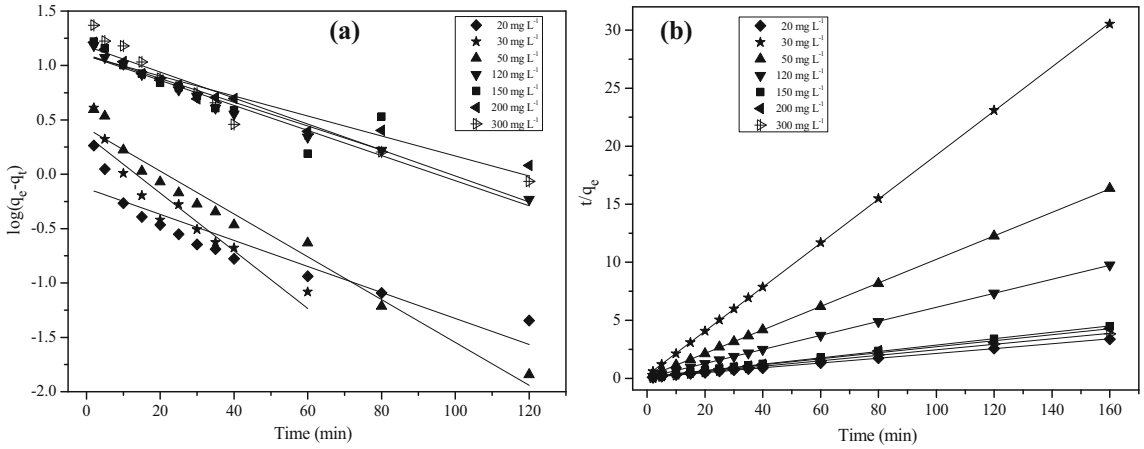

Fig. 12 The kinetic plots, pseudo-first-order (**a**) and pseudo-second-order (**b**) models

$$h = k_2 q_e^2 \tag{18}$$

The intra-particle diffusion model is used by Weber and Morris [69] and the rate constant (k_{int}, mg g^{-1} $min^{-½}$) is given by [41, 67]:

$$q_t = k_{int} t^{1/2} + C \tag{19}$$

C (mg g^{-1}) is the intercept. The relation gives information about the thickness of the boundary layer and the plot of q_t versus $t^{½}$ should yield a straight line passing by the origin if the biosorption process obeys to the intra-particle diffusion model [46, 70].

The kinetic parameters for the biosorption of MB onto *Luffa cylindrica* fiber are calculated and summarized in Table 4 and Fig. 12. We can observe that only the pseudo-second-order model gives the best fit, with low error probability (5.440×10^{-15} to zero), High F values of pseudo-first-order and high adjusted R^2 (0.9964 to 0.9999). Moreover, the calculated biosorption amount q_e (cal) fits well with experimental one q_e (exp).

An intra-particle diffusion model was used to identify the diffusion mechanism. The plots of q_t versus $t^{1/2}$ (Fig. 13), are multi-linear, indicating the existence of three different stages during the biosorption process. The first sharp stage represents the transfer of MB from the solution to the outer surface of the biosorbent; the second gradual stage can be attributed to the penetration of MB into the interlayer of the biosorbent where the intra-particle diffusion is rate limiting. The third stage corresponds to the equilibrium phase and the weak biosorption is ascribed to the residual low MB concentration [70]. The intra-particle diffusion rate constants (k_{int}) are gathered in Table 4. As the initial MB concentration increases, the amount of MB reaching the biosorbent surface increases and the intra-particle diffusion rate increases [40]. It can also be observed that the lines do pass by the origin ($C = 0.737$ to

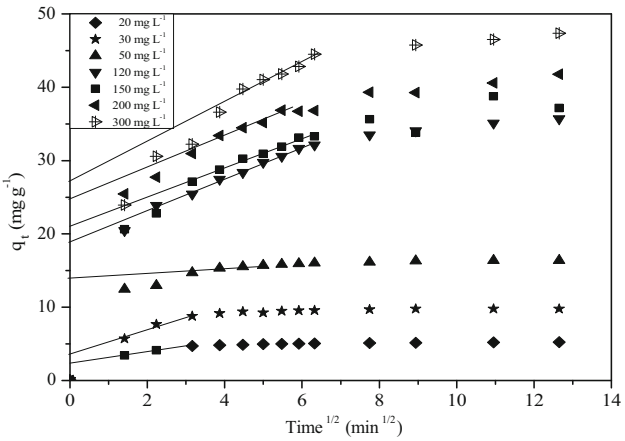

Fig. 13 The intra-particle diffusion model of MB removal by *Luffa cylindrica* fiber at various initial MB concentrations

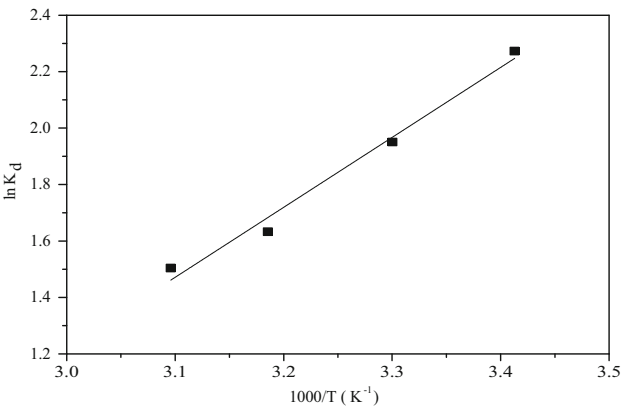

Fig. 14 The Vant Hoff's plot for the determination of thermodynamic parameters

28.789), and this indicates that the transfer mechanism is controlled not only by intra-particle diffusion but also by other mechanisms, such as boundary layer [57]. Similar

Table 5 Thermodynamic parameters for the biosorption of MB onto *Luffa cylindrica* fiber

$\Delta G°$ (kJ mol^{-1})					$\Delta H°$ (kJ mol^{-1})	$\Delta S°$ (kJ mol^{-1} K^{-1})
293 K	303 K	313 K	323 K	333 K		
−5.428	−4.912	−4.396	−3.88	−3.364	−20.547	−0.052

results have been reported for the biosorption of MB onto activated carbons prepared from NaOH-pretreated rice [71], *Luffa cylindrica* fiber-activated carbons [72], sugar beet pulp [21] and low cost biomass material lotus leaf [73].

Thermodynamic studies

The temperature presents a notable effect on the biosorption and the thermodynamic parameters such as change in the standard free energy ($\Delta G°$), standard enthalpy ($\Delta H°$), and standard entropy ($\Delta S°$) are determined [74]:

$$\Delta G^\circ = -RT \ln K_d \tag{20}$$

$$\ln K_d = \frac{-\Delta G^\circ}{RT} = \frac{\Delta S^\circ}{R} - \frac{\Delta H^\circ}{RT} \tag{21}$$

where R is the universal gas constant (8.314 J mol^{-1} K^{-1}), T (K) the absolute temperature and K_d (L g^{-1}) the distribution coefficient for the biosorption calculated from the following relation [27]:

$$K_d = \frac{q_e}{C_e} \tag{22}$$

The plot of ln K_d versus of $1/T$ yields a straight line form; $\Delta H°$ and $\Delta S°$ are calculated from the slope and intercept of the plot, respectively (Fig. 14, Table 5). The negative values of $\Delta G°$ and $\Delta H°$ indicate that the biosorption is spontaneous, exothermic and physical in nature, thus confirming the affinity of the biosorbent toward the MB molecule [75]. The negative entropy $\Delta S°$ reflects the decreased randomness at the solid/solution interface during the MB biosorption [75, 76]. Similar results were reported by Barka et al. [27] and Han et al. [77] where MB was adsorbed on *Scolymus hispanicus* L. and Fallen phoenix tree's leaf, respectively.

Desorption study

Desorption studies help in deciding the mechanism of the biosorption process and recovery of adsorbent for the reuse. The MB desorption on the *Luffa cylindrica* (Fig. 15) is low for the four solvents (<10 %) at 293 K. The undesorbed MB in the biosorbate is due to the complex formation (MB—active site) of the biomass, and hence the inability of the eluting solvent to completely desorb the dye [78].

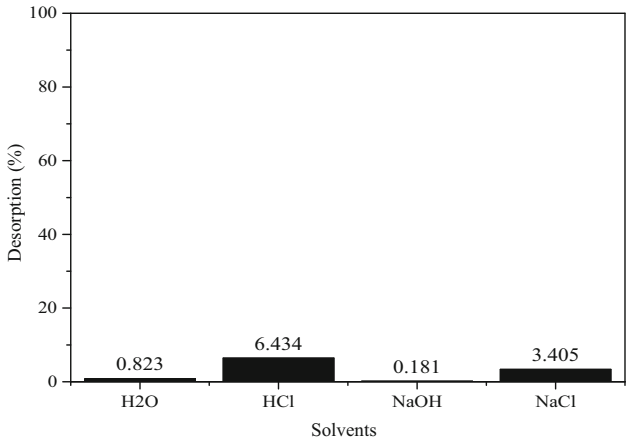

Fig. 15 Batch desorption of MB from biomass using different eluting solvents

Conclusion

The results obtained in the present work showed that the biomass derived from locally available material (*Luffa cylindrica*) can be readily used for the removal of methylene blue from aqueous solutions. In batch studies, the biosorption was strongly dependent on operating parameters such as the contact time, solution pH, particle size, biosorbent dose, initial MB concentration and temperature. The parameters were optimized and the experimental data were analyzed by various isotherm models; the results showed that the isotherm data were well correlated by the Langmuir model. The kinetic studies indicated that the pseudo-second-order model fits suitably the experimental data and suggest that the interlayer diffusion is not the rate-determining step in the MB biosorption mechanism. The maximum monolayer biosorption capacity was found to be 49.46 mg g^{-1} at 20 °C. Moreover, the thermodynamic parameters showed that the biosorption was spontaneous, exothermic and physical in nature. The biosorption experiments indicated that the *Luffa cylindrica* was an efficient biosorbent for the removal of MB and favorably compared with respect to most biomasses reported nowadays.

References

1. Javadian H, Angaji MT, Naushad M (2014) Synthesis and characterization of polyaniline/γ-alumina nanocomposite: a comparative study for the adsorption of three different anionic dyes. J Ind Eng Chem 20:3890–3900
2. Vinod K, Gupta VK, Rajeev Jain R, Arunima Nayak A, Agarwal S, Shrivastava M (2011) Removal of the hazardous dye—Tartrazine by photodegradation on titanium dioxide surface. Mat Sci Eng C 31:1062–1067
3. Mittal A, Mittal J, Malviya A, Gupta VK (2009) Adsorptive removal of hazardous anionic dye ''Congo red" from wastewater using waste materials and recovery by desorption. J Colloid Interface Sci 340:16–26
4. Demirbaş Ö, Turhan Y, Alkan M (2014) Thermodynamics and kinetics of adsorption of a cationic dye onto sepiolite. Desalin Water Treat 1–8
5. Mittal A, Mittal J, Malviya A, Kaur D, Gupta VK (2010) Decoloration treatment of a hazardous triarylmethane dye, Light Green SF (Yellowish) by waste material adsorbents. J Colloid Interface Sci 342:518–527
6. Mittal A, Kaur D, Malviya A, Mittal J, Gupta VK (2009) Adsorption studies on the removal of coloring agent phenol red from wastewater using waste materials as adsorbents. J Colloid Interface Sci 337:345–354
7. Gupta VK, Ali I, Saleh TS, Nayak A, Agarwal S (2012) Chemical treatment technologies for waste-water recycling—an overview. RSC Adv 2:6380–6388
8. Benadjemia M, Millière L, Reinert L, Benderdouche N, Duclaux L (2011) Preparation, characterization and Methylene Blue adsorption of phosphoric acid activated carbons from globe artichoke leaves. Fuel Process Technol 92:203–1212
9. Gupta VK, Jain R, Mittal A, Saleh TA, Nayak A, Agarwal S, Sikarwar S (2012) Photo-catalytic degradation of toxic dye amaranth on TiO2/UV in aqueous suspensions. Mat Sci Eng C 32:12–17
10. Karthikeyan S, Gupta VK, Boopathy R, Titus A, Sekaran G (2012) A new approach for the degradation of high concentration of aromatic amine by heterocatalytic Fenton oxidation: kinetic and spectroscopic studies. J Mol Liq 173:153–163
11. Zhou Q, Gong W, Xie C, Yuan X, Li Y, Bai C, Chen S, Xu N (2011) Biosorption of Methylene Blue from aqueous solution on spent cottonseed hull substrate for Pleurotus ostreatus cultivation. Desalin Water Treat 29:317–325
12. Aksu Z, Ertuğrul S, Dönmez G (2010) Methylene Blue biosorption by Rhizopus arrhizus: effect of SDS (sodium dodecylsulfate) surfactant on biosorption properties. Chem Eng J 158:474–481
13. Saleh TA, Gupta VK (2012) Photo-catalyzed degradation of hazardous dye methyl orange by use of a composite catalyst consisting of multi-walled carbon nanotubes and titanium dioxide. J Colloid Interface Sci 371:101–106
14. Gupta VK, Agarwal S, Saleh TA (2011) Synthesis and characterization of alumina-coated carbon nanotubes and their application for lead removal. J Hazard Mater 185:17–23
15. Gupta VK, Srivastava SK, Mohan D, Sharma S (1998) Design parameters for fixed bed reactors of activated carbon developed from fertilizer waste for the removal of some heavy metal ions. Waste Manag 17:517–522
16. Jain AK, Gupta VK (2003) A comparative study of adsorbents prepared from industrial wastes for removal of dyes. Sep Sci Technol 38:463–481
17. Saleh TA, Gupta VK (2012) Column with CNT/magnesium oxide composite for lead(II) removal from water. Environ Sci Pollut Res 19:1224–1228
18. Guler UA, Sarioglu M (2013) Single and binary biosorption of Cu (II), Ni (II) and methylene blue by raw and pretreated Spirogyra sp.: equilibrium and kinetic modeling. J Environ Chem Eng 1:369–377
19. Mona S, Kaushik A, Kaushik CP (2011) Biosorption of reactive dye by waste biomass of Nostoc linckia. Ecol Eng 37:1589–1594
20. Irem S, Khan QM, Islam E, Hashmat AJ, Ul Haq MA, Afzal M, Mustafa T (2013) Enhanced removal of reactive navy blue dye using powdered orange waste. Ecol Eng 58:399–405
21. Vučurović VM, Razmovski RN, Tekić MN (2012) Methylene blue (cationic dye) adsorption onto sugar beet pulp: equilibrium isotherm and kinetic studies. J Taiwan Inst Chem Eng 43:108–111
22. Deepaa K, Chandran P, Khan SS (2013) Bioremoval of Direct Red from aqueous solution by Pseudomonas putida and its adsorption isotherms and kinetics. Ecol Eng 58:207–213
23. Javadian H, Ahmadi M, Ghiasvand M, Kahrizi S, Katal R (2013) Removal of Cr(VI) by modified brown algae Sargassum bevanom from aqueous solution and industrial wastewater. J Taiwan Inst Chem Eng 44:977–989
24. Daneshvar E, Kousha M, Sohrabi MS, Khataee A, Converti A (2012) Biosorption of three acid dyes by the brown macroalga Stoechospermum marginatum: isotherm, kinetic and thermodynamic studies. Chem Eng J 195–196:297–306
25. Mittal A, Mittal J, Malviya A, Gupta VK (2010) Removal and recovery of Chrysoidine Y from aqueous solutions by waste materials. J Colloid Interface Sci 344:497–507
26. Barka N, Ouzaouit K, Abdennouri M, El Makhfouk M (2013) Dried prickly pear cactus (Opuntia ficus indica) cladodes as a low-cost and eco-friendly biosorbent for dyes removal from aqueous solutions. J Taiwan Inst Chem Eng 44:52–60
27. Barka N, Abdennouri M, Makhfouk MEL (2011) Removal of methylene blue and eriochrome black T from aqueous solutions by biosorption on Scolymus hispanicus L.: kinetics, equilibrium and thermodynamics. J Taiwan Inst Chem Eng 42:320–326
28. Ofomaja AE, Ukpebor EE, Uzoekwe SA (2011) Biosorption of Methyl violet onto palm kernel fiber: diffusion studies and multistage process design to minimize biosorbent mass and contact time. Biomass Bioenergy 35:4112–4123
29. Deniz F, Karaman S, Saygideger SD (2011) Biosorption of a model basic dye onto Pinus brutia Ten.: evaluating of equilibrium, kinetic and thermodynamic data. Desalination 270:199–205
30. Gupta VK, Nayak A (2012) Cadmium removal and recovery from aqueous solutions by novel adsorbents prepared from orange peel and Fe2O3 nanoparticles. Chem Eng J 180:81–90
31. Ncibi MC, Mahjou B, Seffen M (2007) Kinetic and equilibrium studies of methylene blue biosorption by Posidonia oceanica (L.) fibres. J Hazard Mater B139:280–285
32. Suyamboo BK, Srikrishnaperumal R (2014) Biosorption of crystal violet onto cyperus rotundus in batch system: kinetic and equilibrium modeling. Desalin Water Treat 52:4492–4507
33. Belala Z, Jeguirim M, Belhachemi M, Addoun F, Trouvé G (2011) Biosorption of basic dye from aqueous solutions by Date Stones and Palm-Trees Waste: kinetic, equilibrium and thermodynamic studies. Desalination 27:180–187
34. Oboh IO, Aluyor EO, Audu TOK (2011) Application of Luffa Cylindrica in natural form as biosorbent to removal of divalent metals from aqueous solutions -kinetic and equilibrium study. Waste Water-Treat Reutil 195–212
35. Wang LG, Yan GB (2011) Adsorptive removal of direct yellow 161 dye from aqueous solution using bamboo charcoals activated with different chemicals. Desalination 274:81–90
36. Mall ID, Srivastava VC, Kumar GVA, Mishra IM (2006) Characterization and utilization of mesoporous fertilizer plant waste carbon for adsorptive removal of dyes from aqueous solution. Colloids Surf A278:175–187

37. Tanobe VOA, Sydenstricker THD, Munaro M, Amico SC (2005) A comprehensive characterization of chemically treated Brazilian sponge-gourds (Luffa cylindrica). Polym Test 24:474–482
38. Wang Y, Shen XY (2012) Optimum Plasma Surface Treatment of Luffa Fibers. J Macromol Sci Part B: Phys 51:662–670
39. González-García P, Centeno TA, Urones-Garrote E, Ávila-Brande D, Otero-Díaz LC (2013) Microstructure and surface properties of lignocellulosic-based activated carbons. Appl Surf Sci 265:731–737
40. El-Haddad M, Regti A, Slimani R, Lazar S (2014) Assessment of the biosorption kinetic and thermodynamic for the removal of safranin dye from aqueous solutions using calcined mussel shells. J Ind Eng Chem 20:717–724
41. Javadian H, Sorkhrodi FZ, Koutenaei BB (2014) Experimental investigation on enhancing aqueous cadmium removal via nanostructure composite of modified hexagonal type mesoporous silica with polyaniline/polypyrrole nanoparticles. J Ind Eng Chem 20:3678–3688
42. Crini G, Peindy HN, Gimbert F, Robert C (2007) Removal of C.I. Basic Green 4 (malachite green) from aqueous solutions by adsorption using cyclodextrin based adsorbent: kinetic and equilibrium studies. Sep Purif Technol 53:97–110
43. Saeed A, Iqbal M, Zafar IS (2009) Immobilization of Trichoderma viride for enhanced methylene blue biosorption: batch and column studies. J Hazard Mater 168:406–415
44. Han R, Wang Y, Han P, Shi J, Yang J, Lu Y (2006) Removal of methylene blue from aqueous solution by chaff in batch mode. J Hazard Mater B137:550–557
45. Sadaf S, Bhatti HN (2014) Batch and fixed bed column studies for the removal of Indosol Yellow BG dye by peanut husk. J Taiwan Inst Chem Eng 45:541–553
46. Deniz F, Saygideger SD (2010) Equilibrium, kinetic and thermodynamic studies of Acid Orange 52 dye biosorption by Paulownia tomentosa Steud. Leaf powder as a low-cost natural biosorbent. Bioresour Technol 101:5137–5143
47. Mouni L, Merabet D, Bouzaza A, Belkhiri L (2011) Adsorption of Pb(II) from aqueous solutions using activated carbon developed from Apricot stone. Desalination 276:148–153
48. Aksu Z, Karabayir G (2008) Comparison of biosorption properties of different kinds of fungi for the removal of Gryfalan Black RL metal-complex dye. Bioresour Technol 9:7730–7741
49. Çolak F, Atar N, Olgun A (2009) Biosorption of acidic dyes from aqueous solution by Paenibacillus macerans: kinetic, thermodynamic and equilibrium studies. Chem Eng J 150:122–130
50. Khan AA, Ahmad R, KhanA Mondal PK (2013) Preparation of unsaturated polyester Ce(IV) phosphate by plastic waste bottles and its application for removal of Malachite green dye from water samples. Arabian J Chem 6:361–368
51. Aksu Z, Akın AB (2010) Comparison of Remazol Black B biosorptive properties of live and treated activated sludge. Chem Eng J 165:184–193
52. Reddy DHK, Ramana DKV, Seshaiah K, Reddy AVR (2011) Biosorption of Ni (II) from aqueous phase by Moringa oleifera bark, a low cost biosorbant. Desalination 268:150–157
53. Vijayaraghavan K, Padmesh TVN, Palanivelu K, Velan M (2006) Biosorption of nickel (II) ions onto Sargassum wightii: application of two-parameter and three-parameter isotherm models. J Hazard Mater B133:304–308
54. Ghasemi M, Khosroshahy MZ, Abbasabadi AB, Ghasemi N, Javadian H, Fattahi M (2015) Microwave-assisted functionalization of Rosa Canina-L fruits activated carbon with tetraethylenepentamine and its adsorption behavior toward Ni(II) in aqueous solution: kinetic, equilibrium and thermodynamic studies. Powder Technol 274:362–371
55. Javadian H, Ghorbani F, Tayebi HA, Asl SMH (2015) Study of the adsorption of Cd (II) from aqueous solution using zeolite-based geopolymer, synthesized from coal fly ash; kinetic, isotherm and thermodynamic studies. Arabian J Chem 8:837–849
56. Wang L (2012) Application of activated carbon de rived from 'waste' bamboo culms for the adsorption of azo disperse dye: kinetic, equilibrium and thermodynamic studies. J Environ Manag 102:79–87
57. Demir H, Top A, Balköse D, Ülkü S (2008) Dye adsorption behavior of Luffa cylindrica fiber. J Hazard Mater 153:389–394
58. Gürses A, Hassani A, Kıranşan M, Açışlı ö, Karaca S (2014) Removal of methylene blue from aqueous solution using by untreated lignite as potential low-cost adsorbent: kinetic, thermodynamic and equilibrium approach. J Water Process Eng 2:10–21
59. Abdelwahab O (2008) Evaluation of the use of loofa activated carbons as potential adsorbents for aqueous solutions containing dye. Desalination 222:357–367
60. Altınışık A, Gür E, Seki Y (2010) A natural sorbent, Luffa cylindrica for the removal of a model basic dye. J Hazard Mater 179:658–664
61. Albadarin AB, Mangwandi C (2015) Mechanisms of Alizarin Red S and Methylene blue biosorption onto olive stone by-product: isotherm study in single and binary systems. J Environ Manag 164:86–93
62. Sarat Chandra T, Mudliar SN, Vidyashankar S, Mukherji S, Sarada R, Krishnamurthi S, Chauhan VS (2015) Defatted algal biomass as a non-conventional low-cost adsorbent: surface characterization and methylene blue adsorption characteristics. Bioresour Technol 184:395–404
63. Ghaedi M, Kokhdan MN (2015) Removal of methylene blue from aqueous solution by wood millet carbon optimization using response surface methodology. Spectrochim Acta A 136:141–148
64. Ghaedi M, Golestani Nasab A, Khodadoust S, Rajabi M, Azizian S (2014) Application of activated carbon as adsorbents for efficient removal of methylene blue: kinetics and equilibrium study. J Ind Eng Chem 20:2317–2324
65. Lagergren S (1898) Zur theorie der sogenannten adsorption gelöster stoffe. Kungliga Svenska Vetenskapsakademiens Handlingar 24:1–39
66. Javadian H, Koutenaei BB, Shekarian E, Sorkhrodi FZ, Khatti R, Toosi MR (2014)Application of functionalize d nano HMS type mesoporous silica with N-(2-ami noethyl)-3-a minopropyl methyldimeth oxysilan e as a suitable adsorbent for removal of Pb(II) from aqueous media and industrial wastewater. J Saudi Chem Soc xxx xxx–xxx
67. Javadian H, Taghavi M (2014) Application of novel Polypyrrole/thiol-functionalized zeolite Beta/MCM-41 type mesoporous silica nanocomposite for adsorption of Hg2+ from aqueous solution and industrial wastewater: kinetic, isotherm and thermodynamic studies. Appl Surf Sci 289:487–494
68. Javadian H, Vahedian P, Toosi MR (2013) Adsorption characteristics of Ni(II) from aqueous solution and industrial wastewater onto Polyaniline/HMS nanocomposite powder. Appl Surf Sci 284:13–22
69. Weber WJ, Morris JC (1963) Kinetics of adsorption on carbon from solution. J Sanit Eng Div Am Soc Civ Eng 89:31–59
70. Akar E, Aylinşik A, Seki Y (2013) Using of activated carbon produced from spent tea leaves for the removal of malachite green from aqueous solution. Ecol Eng 52:19–27
71. ChenY Zhai SR, Liu N, Song Y, An QD, Song XW (2013) Dye removal of activated carbons prepared from NaOH-pretreated rice husks by low-temperature solution-processed carbonization and H3PO4 activation. Bioresour Technol 144:401–409
72. Cherifi H, Bentahar F, Hanini S (2013) Kinetic studies on the adsorption of methylene blue onto vegetal fiber activated carbons. Appl Surf Sci 282:52–59

73. Han X, Wang W, Ma X (2011) Adsorption characteristics of methylene blue onto low cost biomass material lotus leaf. Chem Eng J 171:1–8
74. Hu Z, Chen H, Ji F, Yuan S (2010) Removal of Congo Red from aqueous solution by cattail root. J Hazard Mater 173:292–297
75. Rehman MSU, Kim I, Han JI (2012) Adsorption of methylene blue dye from aqueous solution by sugar extracted spent rice biomass. Carbohydr Polym 90:1314–1322
76. Albadarin AB, Mangwandi C, Al-Muhtaseb AH, Walker GM, Allen SJ, Ahmad MNM (2012) Kinetic and thermodynamics of chromium ions adsorption onto low-cost dolomite adsorbent. Chem Eng J 179:193–202
77. Han R, Zou W, Yu W, Cheng S, Wang Y, Shi J (2007) Biosorption of methylene blue from aqueous solution by fallen phoenix tree's leaves. J Hazard Mater 141:156–162
78. Oladoja NA, Aboluwoye CO, Akinkugbe AO (2009) Evaluation of loofah as a sorbent in the decolorization of basic dye contaminated aqueous system. Ind Eng Chem Res 48:2786–2794